Hindawi Publishing Corporation
Advances in Materials Science and Engineering
Volume 2016, Article ID 6465983, 13 pages
http://dx.doi.org/10.1155/2016/6465983

Research Article

Coal and Gangue Underground Pneumatic Separation Effect Evaluation Influenced by Different Airflow Directions

Kehong Zheng,[1,2] Changlong Du,[1] Jianping Li,[1] and Bingjing Qiu[1]

[1] *College of Mechanical and Electrical Engineering, China University of Mining and Technology, Xuzhou 221116, China*
[2] *Department of Metallurgical Engineering, College of Mines and Earth Sciences, University of Utah, Salt Lake City, UT 84112-0114, USA*

Correspondence should be addressed to Kehong Zheng; zkhcumt@gmail.com

Received 23 June 2015; Accepted 9 November 2015

Academic Editor: Charles C. Sorrell

Coal and gangue underground pneumatic separation is of key importance for green mining. Two kinds of arrangement schemes for high-pressure value used in pneumatic separation system are proposed in this study. Pneumatic separation effects are examined under different arrangement of high-pressure value. Here, theoretical pneumatic separation distance formulas of mineral particles affected by different airflow directions are derived and validated by a series of numerical simulations and orthogonal experiments. In the following analysis, the effects of gangue diameter (d), conveyor velocity (v_0), and the height difference between conveyor belt and air nozzle (h_p) are mainly considered. The numerical simulation and experimental results indicate that pneumatic separation effects under the condition of u and v_0 being in the opposite direction will be better than that of u and v_0 being in the same direction. The pneumatic separation distance ΔS shows a decreasing trend with the increasing of the three factors. The study also shows that gangue diameter has the most significant influence on separation distance, followed by conveyor velocity v_0 and height difference h_p.

1. Introduction

Coal has been regarded as the most widely used fuel in many countries because of the lack of oil and gas resources, which is expected to be prolonged over decades. Initial underground separation for coal and gangue is an indispensable process of mine production and has great significance for coal preparation. Gangue from underground separation can be used for filling mined-out areas, improving the quality of raw coal, decreasing the cost of preparation, saving transport capacity, and reducing the amount of waste polluting the environment above the ground [1, 2]. Currently, several technologies of underground separation coal and gangue are proposed, which include an automated hydraulic separation technology and a rotating impact method of coal gangue separation underground [3–6]. However, underground separation technologies mentioned above have the disadvantages of high cost, being time-consuming, and low automation.

With the development of digital image processing technology, scholars mainly probed into a general machine vision approach for online identification of coal and gangue [7–10]. The influences of camera location, particle overlap, image blur degree, and conveyor velocity were investigated during the coal and gangue particles online transportation [11–14]. From the above discussion, machine vision process has the advantages of real-time processing, lower cost, and higher intelligence.

Lots of researches have conducted the online identification of coal and gangue, which have proved the feasibility of image recognition of coal and gangue. Nevertheless, pneumatic separation of coal and gangue has not been discussed adequately and has not been applied in mineral separation.

Currently, pneumatic separation has been widely used in agriculture field and rare metal recycling field. A cotton seed online separation system based on machine vision was designed to realize automatic separation of red-brown and black cotton seed by compressed airflow in the air [15]. Guo et al. proposed a series of methods to realize the recycling of printed circuit boards (PCBs); the whole process that

involves crushing and electrostatic and pneumatic separation has formed a closed cycle that can return material and provide salable product [16]. Xu et al. described an effective mechanical process including impact crushing from printed circuit boards and investigated the pneumatic separation for metal recovery scraps [17]. Kumar et al. report a simple and eco-friendly physical pneumatic separation process for the recycling of metallic values from PCBs [18, 19]. The effect of orifices on spherical particles was clarified by Hayashi and Oki through numerical simulations of air-solid multiphase flow in a vertical single-column pneumatic separator to realize recycle important rare metals (such as tantalum) in the PCBs of waste electronic equipment [20]. Havlik et al. focused on studying mechanical-physical pretreatment of PCBs from used consumer equipment followed by extraction of copper and tin from residue fractions by leaching in hydrochloric acid solutions [21].

Moreover, researchers also have done lots of research on pneumatic separation of coal particles (particle size, i.e., mainly less than 5 mm) in fluidized conveyor. Liu et al. investigated the pneumatic classification behavior in a laboratory CCMC reactor with such a configuration by removing the coal fraction below a given size (e.g., 3.0 mm) from 0 to 20.0 mm [22, 23]. Yang et al. attempted to carry out a systematic process analysis of fine coal preparation in a vibrated gas-fluidized bed (VGFB) [24].

The research group has proved the feasibility of pneumatic separation technology for coal and gangue, yet pneumatic separation effects influenced by different arrangements of high-pressure value have not been presented. In this paper, theoretical models were established for the study of pneumatic separation process affected by different high-pressure airflow direction. Then, a series of numerical simulations and orthogonal experiments were conducted to evaluate the separation effect under different airflow direction. Finally, the theoretical models were corrected based on experiment data.

2. Principle

Underground coal and gangue pneumatic separation system, which is shown in Figure 1, contains three parts: preliminary crush separation system, machine version system, and pneumatic separation system. Preliminary crush separation system mainly contains roll-type crusher, spiral size screen, and several conveyor belts, which aims to limit the granularity of coal and gangue sent into machine vision system within a range of 50 mm~100 mm. Machine vision system is a highly automated technology using digital image processing technology to identify the size and location of gangue based on identification algorithms; then the identified information will be sent to pneumatic separation system through image sensor. Pneumatic separation system is controlled by computer to realize coal and gangue pneumatic separation.

Two kinds of arrangement schemes for high-pressure value used in pneumatic separation system are presented in Figure 1. One is that particles' motion direction is the same as that of high-pressure airflow; the other is that particles' motion direction is opposite to that of high-pressure airflow. As shown in Figure 1, the high-pressure values 12(a) are

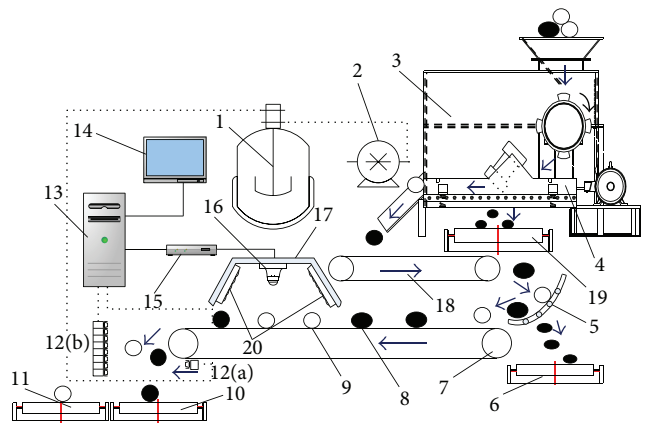

Figure 1: Separation system of coal and gangue. (1) High-pressure gasholder; (2) air compressor; (3) separation equipment; (4) vibrating sieve; (5) sieve plate; (6) coal conveyor belt; (7) conveyer belt for coal and gangue recognition; (8) coal; (9) gangue; (10, 11) materials conveyor belt; (12) (a, b) high-pressure value array; (13) control equipment; (14) computer; (15) image acquisition equipment; (16) CCD camera; (17) camera box; (18) conveyor belt; (19) coal conveyor belt; (20) LED light array.

arranged under the conveyor belt (7) in the first arrangement scheme, mixed mineral materials are thrown from conveyor belt (7), coal materials unaffected by high-pressure airflow will fall onto conveyor belt (10), and gangue materials affected by high-pressure airflow will fall onto conveyor belt (11). In the second arrangement scheme, high-pressure values 12(b) are arranged in front of conveyor belt (7), mixed mineral materials are thrown from conveyor belt (7), coal materials unaffected by high-pressure airflow will fall on conveyor belt (11), and gangue materials affected by high-pressure airflow will fall on conveyor belt (10).

3. Model Development

3.1. Theoretical Model. The movement of mineral materials affected by high-pressure airflow can be divided into three stages: (1) particle's movement before falling into airflow domain; (2) movement of particle in airflow domain; (3) movement of particle after leaving the airflow domain. When the movement direction of mineral materials is the same as that of high-pressure airflow, coal particle trajectory unaffected by high-pressure airflow is shown in Figure 2(a) of curve 1 and gangue particle trajectory affected by high-pressure airflow is shown in Figure 2(a) of curve 2. When the movement direction of mineral materials is opposite to that of high-pressure airflow, coal particle trajectory unaffected by high-pressure airflow is shown in Figure 2(b) of curve 1 and gangue particle trajectory affected by high-pressure airflow is shown in Figure 2(b) of curve 2.

As shown in Figure 2, ΔS represents the pneumatic separation distance of coal and gangue, h_p represents the height difference between gangue mass center on conveyor belt and upper boundary of the airflow domain, t_p represents the motion time before gangue came into the airflow domain, $v_{p1,2}$ is the velocity in direction y of gangue before falling

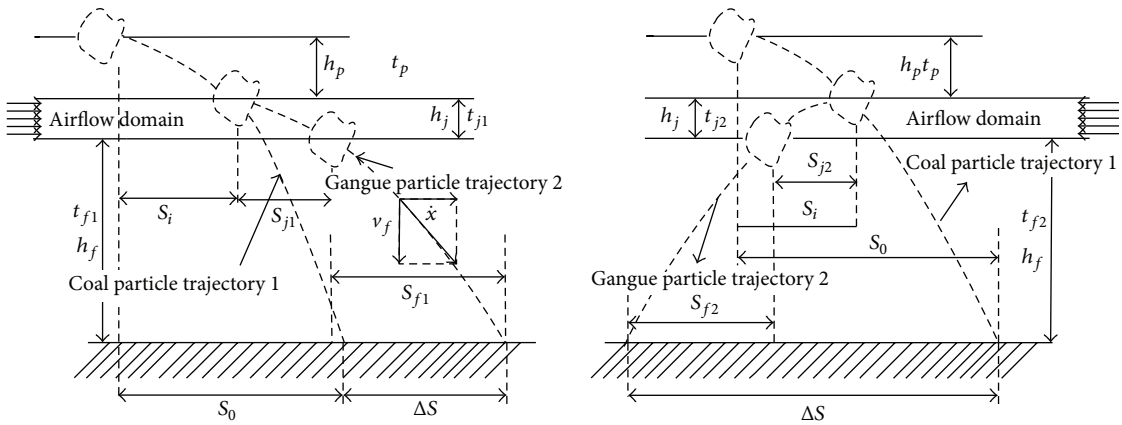

(a) $\dot{x}$ and u are in the same direction

(b) $\dot{x}$ and u are in the opposite direction

Figure 2: Pneumatic separation model of coal and gangue.

into airflow domain, and h_j represents the height of airflow domain. S_i represents the displacement in x direction of gangue before entering airflow domain. $t_{j1,2}$ represents the motion time of gangue in airflow domain, and S_j represents the motion displacement in x direction of gangue in airflow domain. $v_{f1,2}$ represents the motion velocity in y direction of gangue in airflow domain, $\dot{x}(t_{j1,2})$ represents the motion velocity in x direction of gangue in airflow domain, $t_{f1,2}$ represents the motion time of gangue after leaving airflow domain, and $S_{f1,2}$ represents the motion displacement in x direction of gangue after leaving airflow domain. In the following equations, subscript 1 is used to represent when airflow velocity and conveyor belt velocity are in the same direction, and subscript 2 is used to represent when airflow velocity and conveyor belt velocity are in the opposite direction.

Coal and gangue materials will be recognized by machine vision system and the recognized image information will be sent to pneumatic separation system through image sensor. Coal particles will fall from the conveyor belt freely without the effect of high-pressure airflow. When the motion direction of mineral materials is the same as that of high-pressure airflow, gangue material will change its trajectory and will be thrown significantly farther than that of coal particle. When the motion direction of mineral materials is opposite to that of high-pressure airflow, gangue material will change its trajectory to an opposite direction compared with that of coal particle. The motions of coal and gangue particles are analyzed, respectively, in the following three sections.

When coal materials are recognized by machine vision system, coal particles will fall from the conveyor belt freely unaffected by high-pressure airflow. t_0 and S_0 can be obtained through (1) and (2). Gangue motion law at this stage is the same as coal materials. S_i and v_p can be also shown by (3) and (4), where t_0 represents the motion time of coal particle, and S_0 represents the displacement of coal particle in x direction:

$$t_0 = \sqrt{\frac{2\left(h_p + h_j + h_f\right)}{g}}, \tag{1}$$

$$S_0 = v_0\sqrt{\frac{2\left(h_p + h_j + h_f\right)}{g}}, \tag{2}$$

$$S_i = v_0\sqrt{\frac{2h_p}{g}}, \tag{3}$$

$$v_p = g\sqrt{\frac{2h_p}{g}}. \tag{4}$$

In order to calculate the acting force of high pressure on gangue particles, multiple rectangular polyline is used to approximate gangue particle's physical shape if the dynamic pressure head of the airflow domain is known in special location. The acting force of high-pressure airflow on gangue can be presented by

$$F = \iint_A P_d\, dA = \sum_{i=1}^{m} P_{di} A_i, \tag{5}$$

where F represents the acting force of the high airflow on gangue, P_{di} represents the high pressure in ring i, A_i represents the area of ring i, and m represents the total number of rings.

As shown in Figure 3, gangue is affected by airflow with different directions. In order to analyze the movement of gangue particle in high-pressure airflow domain, air resistance and horizontal momentum's increment of airflow domain are ignored. The theoretical formula of gangue displacement in direction y can be expressed as $s = \int_0^{t_{j1,2}} (v_p + g t_{j1,2}) dt = h - d$; then $t_{j1,2}$ can be obtained as shown in

$$t_{j1,2} = \frac{\sqrt{v_p^2 + 2g\left(h - d\right)} - v_p}{g}. \tag{6}$$

As shown in (6), gangue affected by different airflow direction has the same motion time in airflow domain. Gangue will be affected by two forces after falling into high-pressure airflow domain. The two forces applied on gangue

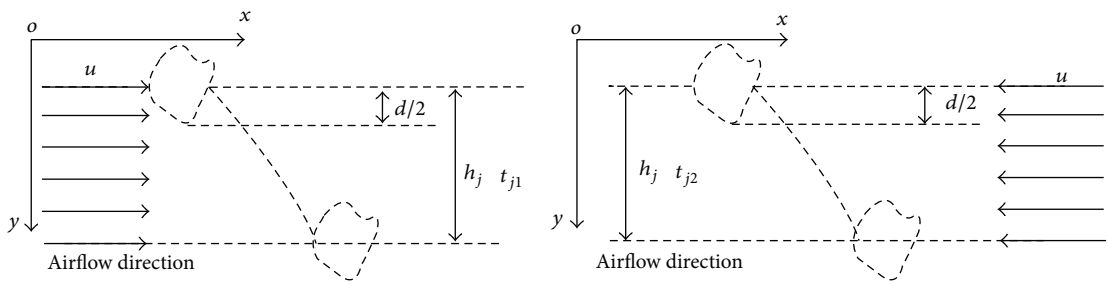

(a) $\dot{x}$ and u are in the same direction

(b) $\dot{x}$ and u are in the opposite direction

Figure 3: Schematic diagram of gangue's motion in airflow domain.

particle are gravity and high dynamic pressure. Airflow dynamic pressure will convert to static pressure on condition that the velocity of airflow u is larger than gangue's horizontal velocity v_0 and airflow must keep dynamic pressure $p_d = \rho\dot{x}^2/2$. The pressure difference can be expressed as $\Delta p_d = \rho(u^2 - \dot{x}^2)/2$. According to (5), the formula of airflow force can be expressed by

$$F = \iint p\,dA \approx \sum_i p_i A_i = \frac{1}{2}\rho \sum_i \left(u_i^2 - \dot{x}^2\right) A_i. \tag{7}$$

When the curvature of gangue surface is not too large, it can be approximately seen as a plane, so $\forall u_i = u$, (7) can be changed to

$$F = \frac{1}{2}\rho\left(u^2 - \dot{x}^2\right) A. \tag{8}$$

According to Newton's second law, (8) can be changed to

$$\begin{aligned} m\ddot{x} &= \frac{1}{2}\rho A\left(u^2 - \dot{x}^2\right), \\ &\qquad \dot{x} \text{ and } u \text{ are in same direction}, \\ m\ddot{x} &= -\frac{1}{2}\rho A\left(u^2 + \dot{x}^2\right), \\ &\qquad \dot{x} \text{ and } u \text{ are in opposite direction}. \end{aligned} \tag{9}$$

As shown in (9), the expressions are corresponding to different airflow directions. The general solution of displacement in x direction of gangue moving in the airflow can be obtained by taking Laplace transform to (9), and the result is shown in

$$\begin{aligned} x\left(t_{j1}\right) &= \frac{A\rho C_2 + m\ln\left(e^{(2C_1u - At_{j1}\rho u)/m} + 1\right) - mC_1 + At_{j1}\rho u}{A\rho}, \\ &\qquad \dot{x} \text{ and } u \text{ are in same direction}, \\ x\left(t_{j2}\right) &= \frac{A\rho C_4 + 2m\ln\left(\cos\left(\left(At_{j2}u\rho - 2muC_3\right)/2m\right)\right)}{A\rho}, \\ &\qquad \dot{x} \text{ and } u \text{ are in opposite direction}. \end{aligned} \tag{10}$$

The velocity of gangue in x direction in airflow domain can be obtained by taking derivation of (10). The general solution is shown in

$$\begin{aligned} x'\left(t_{j1}\right) &= \frac{ue^{At_{j1}u\rho/m}}{e^{2C_1u/m} + e^{At_{j1}u\rho/m}}, \\ &\qquad \dot{x} \text{ and } u \text{ are in same direction}, \\ x'\left(t_{j2}\right) &= -u\tan\left(\frac{At_{j2}\rho u - 2muC_3}{2m}\right), \\ &\qquad \dot{x} \text{ and } u \text{ are in opposite direction}. \end{aligned} \tag{11}$$

In order to calculate the constant coefficients C_1, C_2, C_3, and C_4 in (10), the initial constraint conditions are as follows: the initial position of the gangue is $x(0) = 0$ and the initial velocity of gangue is $x'(0) = v_0$.

When $\dot{x}$ and u are in the same direction, the general solution of $x(t_j)$ and $x'(t_j)$ can be obtained by (10) and (11). C_1 and C_2 are shown in

$$\begin{aligned} C_1 &= \frac{m\ln\left(u/v_0 - 1\right)}{2u}, \\ C_2 &= \frac{m^2\ln\left(u/v_0 - 1\right) - 2mu\ln\left(u/v_0\right)}{2Au\rho}. \end{aligned} \tag{12}$$

The general solutions of $x(t_j)$ and $x'(t_j)$ are shown in

$$\begin{aligned} x\left(t_{j1}\right) &= \frac{m\ln\left(e^{(m\ln(u/v_0-1) - At_{j1}\rho u)/m} + 1\right) - 2mu\ln\left(u/v_0\right) + At_{j1}\rho u}{2A\rho u}, \\ x'\left(t_{j1}\right) &= \frac{ue^{At_{j1}u\rho/m}}{e^{\ln(u/v_0-1)} + e^{At_{j1}u\rho/m}}. \end{aligned} \tag{13}$$

When $\dot{x}$ and u are in the opposite direction, the general solution of $x(t_j)$ and $x'(t_j)$ can be obtained by (10) and (11). C_3 and C_4 are shown by

$$\begin{aligned} C_3 &= \frac{\arccos\left(u/\sqrt{v_0^2 + u^2}\right)}{u}, \\ C_4 &= \frac{-2m\ln\left(u/\sqrt{v_0^2 + u^2}\right)}{A\rho}. \end{aligned} \tag{14}$$

The general solutions of $x(t_j)$ and $x'(t_j)$ are shown by (15) and (16), respectively,

$$x\left(t_{j2}\right) = \frac{2m\ln\left(\cos\left(\left(At_{j2}u\rho - 2m\arccos\left(u/\sqrt{v_0^2+u^2}\right)\right)/2m\right)\right) - 2m\ln\left(u/\sqrt{v_0^2+u^2}\right)}{A\rho}, \tag{15}$$

$$x'\left(t_{j2}\right) = -u\tan\left(\frac{At_{j2}\rho u - 2m\arccos\left(u/\sqrt{v_0^2+u^2}\right)}{2m}\right). \tag{16}$$

When gangue particles left the boundary of airflow domain, gangue particles would do flat parabolic motion. The formula of velocity v_f in direction y is shown in

$$v_{f1,2} = \int_0^{t_{j1,2}} \left(v_p + gt\right) dt. \tag{17}$$

$t_{f1,2}$ can be solved through (18) and the result is shown by (19):

$$\begin{aligned} h_f &= \int_0^{t_{f1,2}} \left(v_f + gt\right) dt \\ &= \int_0^{t_{f1,2}} gt\, dt + \int_0^{t_{f1,2}} \int_0^{t_j} \left(v_p + gt\right) d^2t, \end{aligned} \tag{18}$$

$$t_{f1,2} = \frac{-gt_{j1,2}^2 - 2t_{j1,2}v_p + \sqrt{8gh_f + \left(gt_{j1,2}^2 + 2t_{j1,2}v_p\right)^2}}{2g}. \tag{19}$$

The displacement $S_{f1,2}$ of gangue in direction x after leaving the airflow domain can be expressed by

$$S_{f1,2} = x'\left(t_{j1,2}\right) t_{f1,2}. \tag{20}$$

To sum up, when $\dot{x}$ and u are in the same direction, the separation distance ΔS can be calculated by

$$\begin{aligned} \Delta S = S_i + S_{j1} + S_{f1} - S_0 &= v_0\sqrt{\frac{2h_p}{g}} \\ &+ \frac{m\ln\left(e^{(m\ln(u/v_0-1) - At_{j1}\rho u)/m} + 1\right) - 2mu\ln\left(u/v_0\right) + At_{j1}\rho u}{2A\rho u} \\ &+ \frac{2h_f u e^{At_{j1}u\rho/m}}{\left(e^{\ln(u/v_0-1)} + e^{At_{j1}u\rho/m}\right)\left(gt_{j1} + 2v_p\right)t_{j1}} \\ &- v_0\sqrt{\frac{2\left(h_p + h_j + h_f\right)}{g}}. \end{aligned} \tag{21}$$

When $\dot{x}$ and u are in the opposite direction, the separation distance ΔS can be obtained by

$$\begin{aligned} \Delta S &= S_0 + S_{j2} + S_{f2} - S_i \\ &= v_0\sqrt{\frac{2\left(h_p + h_j + h_f\right)}{g}} + \frac{2m\ln\left(\cos\left(\left(At_{j2}u\rho - 2m\arccos\left(u/\sqrt{v_0^2+u^2}\right)\right)/2m\right)\right) - 2m\ln\left(u/\sqrt{v_0^2+u^2}\right)}{A\rho} \\ &+ \tan\left(\frac{At_{j2}\rho u - 2m\arccos\left(u/\sqrt{v_0^2+u^2}\right)}{2m}\right)\frac{2uh_f}{t_{j2}\left(gt_{j2} + 2v_p\right)} - v_0\sqrt{\frac{2h_p}{g}}. \end{aligned} \tag{22}$$

The separation distance ΔS is shown by (21) and (22), which reflects the basic motion law of gangue when influenced by airflow field under different airflow directions. For the limitation of assumption, there exist big differences between theoretical model and practical model. In order to simplify the calculation and correct the difference between theoretical value and practical value, parameters k_n (nonlinear correction factor) and k_r (linear correction factor) are introduced. k_n reflects the convergence rate of the fitting function, and k_r reflects the convergent gain and is used to adjust the fitting effect of formula based on experimental value. Theoretical value will get close to experiment value by adjusting the value of k_n and k_r. The modified formulas with the correction factors are shown in

$$\begin{aligned}\Delta S &= S_i + S_{j1} + S_{f1} - S_0 \\ &= v_0\sqrt{\frac{2h_p}{g}} + \frac{m\ln\left(e^{(m\ln(u/v_0-1)-Ak_nt_{j1}\rho u)/m}+1\right) - 2mu\ln\left(u/v_0\right) + At_{j1}\rho u}{2A\rho u} \\ &\quad + \frac{2h_f u e^{Ak_nt_{j1}u\rho/m}}{\left(e^{\ln(u/v_0-1)}+e^{Ak_nt_{j1}u\rho/m}\right)\left(gt_{j1}+2v_p\right)t_{j1}} - v_0\sqrt{\frac{2\left(h_p+h_j+h_f\right)}{g}} - k_r,\end{aligned} \tag{23}$$

$$\begin{aligned}\Delta S &= S_0 + S_j + S_f - S_i \\ &= v_0\sqrt{\frac{2\left(h_p+h_j+h_f\right)}{g}} + \frac{2m\ln\left(\cos\left(\left(Ak_nt_ju\rho - 2m\arccos\left(u/\sqrt{v_0^2+u^2}\right)\right)/2m\right)\right) - 2m\ln\left(u/\sqrt{v_0^2+u^2}\right)}{A\rho} \\ &\quad + \tan\left(\frac{At_j\rho u - 2m\arccos\left(u/\sqrt{v_0^2+u^2}\right)}{2m}\right)\frac{2uh_f}{t_j\left(gt_j+2v_p\right)} - v_0\sqrt{\frac{2h_p}{g}} - k_r.\end{aligned} \tag{24}$$

3.2. Air-Solid Multiphase Pneumatic Separation Simulation. In order to evaluate the pneumatic separation effect under two kinds of arrangement schemes for high-pressure value, a "fixed coarse-grid" fluid scheme is applied in PFC3D for pneumatic separation simulations. In the fluid scheme, 550 ($22 \times 5 \times 5$: x, y, and z directions) fluid cells are created in a rectangular space ($x = [0, 7000\,\text{mm}]$, $y = [-400\,\text{mm}, 400\,\text{mm}]$, and $z = [300\,\text{mm}, 400\,\text{mm}]$), which covers the rectangular space. A pneumatic boundary should be set for the fluid grid. Driving forces from the fluid flow are applied to the particles as body forces. These forces are also added to the fluid equations and cause change in momentum, as reflected by the change in the pressure gradient in the flow direction.

As shown in Figures 4(a) and 4(b), two available models are established to reduce the computation time without loss in accuracy. The gangue hopper, containing 300 balls, is built at the top right of conveying belt 1; it is aimed at reducing the computation time. The front view of the simulation models at an initial stage under different airflow directions is shown in Figures 4(a) and 4(b), respectively.

In Figure 4(a), the velocity v_0 of conveyor belt 1 and airflow velocity u are in opposite directions. When gangue falls into the airflow domain, gangue particle will change its trajectory to an opposite direction and fall onto conveyor belt 2. The conveyor belt 2 has the same movement direction as airflow velocity; finally gangue particles will be transported to collecting box by conveyor belt 2. In Figure 4(b), conveyor belt v_0 and airflow velocity u are in the same direction. When gangue falls into the airflow domain, gangue particle will throw much farther and fall on conveyor belt 2. The motion of conveyor belt 2 has the same motion direction as conveyor belt 1; finally the gangue particles are transported to collecting box by conveyor belt 2.

In the fluid scheme, a pneumatic boundary is set for two available models. During the simulations, an approximation is made by specifying the velocity boundary at the right end of the model and a pressure boundary as 0.0 Pa at left end with $x = 0\,\text{mm}$. The slip boundary, in which the fluid velocity parallel to the wall surface is nonzero at the wall surface, is specified at the surrounding four walls. In simulation as shown by Figure 4(b), an approximation is made by specifying the velocity boundary at the left end of model and a pressure boundary as 0.0 Pa at the right end with $x = 7000\,\text{mm}$. The initial setup of the slip boundary in Figure 4(b) is the same as that shown in Figure 4(a) and material properties are shown in Table 1.

As shown in Figure 4(a), airflow is injected with a velocity of 300 m/s from the negative direction of x at the starting point, while, in Figure 4(b), air is injected from the positive direction of x. When the pneumatic boundaries are applied at the initial stage, the two side walls applied to confine the assembly are removed simultaneously. Figure 5 shows the front view of simulation result from the initial stage to 1 sec.

It can be obtained from Figure 5 that gangue particles have different motion trajectories under different airflow velocity. As shown in Figures 5(a) and 5(b), gangue particles will do horizontal projectile motion before entering airflow domain, as can be seen at $t = 0.2$ s and $t = 0.4$ s. As shown in Figure 5(a), velocities of conveyor belt 1 v_0 and airflow u are in the opposite direction, and gangue particles will change their motion trajectories to an opposite direction compared with that of coal without the effect of airflow, which can be seen at $t = 0.6$ s, $t = 0.8$ s, and $t = 1.0$ s. As shown in Figure 5(b), velocities of the conveyor belt 1 v_0 and airflow u are in the same direction, and gangue particles will be blown much farther than that of coal without being affected by airflow, as can be seen at $t = 0.6$ s, $t = 0.8$ s, and $t = 1.0$ s.

As can be seen in Figures 5(a) and 5(b), gangue particles will change their trajectories in area A and area C. Areas B and D, as shown in Figures 5(a) and 5(b), illustrated that gangue particles with smaller diameters can be blown much farther.

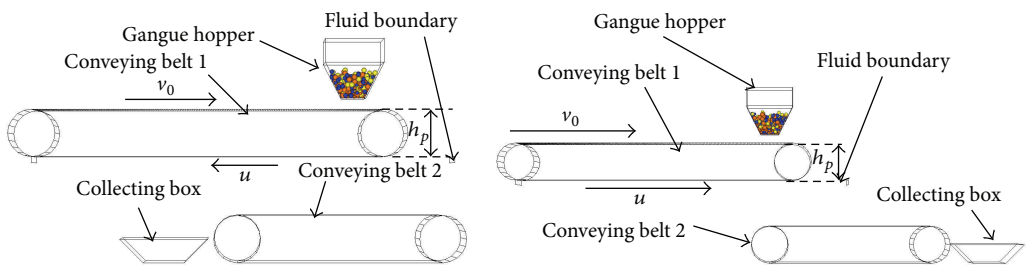

(a) v_0 and u in the opposite direction (b) v_0 and u in the same direction

Figure 4: Air-solid multiphase pneumatic separation.

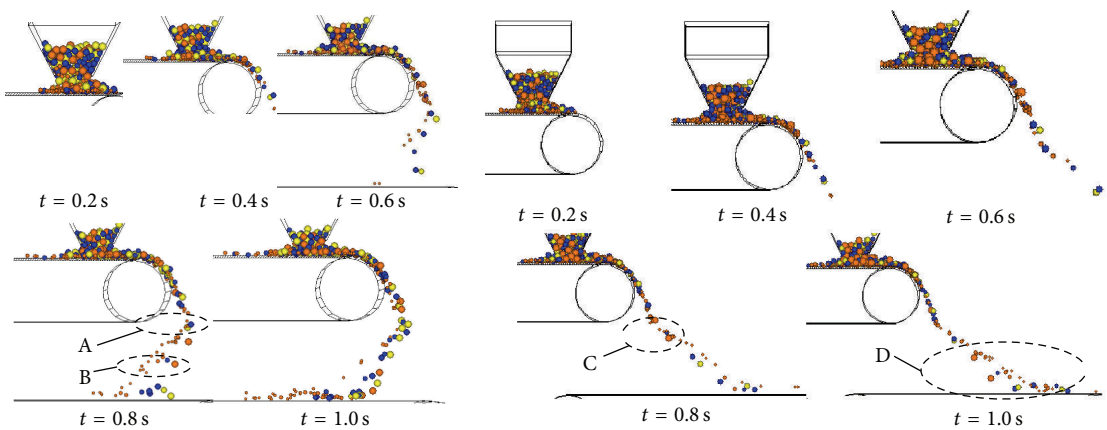

(a) v_0 and u are in the opposite direction (b) v_0 and u are in the same direction

Figure 5: Front view (initial stage to 1 sec; apparent velocity, ±260 m/s).

Table 1: Materials properties.

Parameter	Value	Units
	Ball	
Diameter	50~100	mm
Number	300	—
Density	2700	kg/m^3
Normal stiffness	1×10^6	N/m
Shear stiffness	1×10^6	N/m
Friction coefficient	0.7	—
	Air	
Density	1.205	kg/m^3
Viscosity	1.8×10^{-6}	Pa·s
	Wall	
Normal stiffness	1×10^6	N/m
Shear stiffness	1×10^6	N/m
Friction coefficient	0.3	—

In order to study the pneumatic separation distance influenced by different airflow directions, airflow velocities ±300 m/s are chosen for the research of separation effect. Conveyor velocity v_0 and height difference h_p between conveyor belt and air nozzle are kept constant. The relationships between separation distances and particle diameters under different airflow velocity directions are shown in Figure 6.

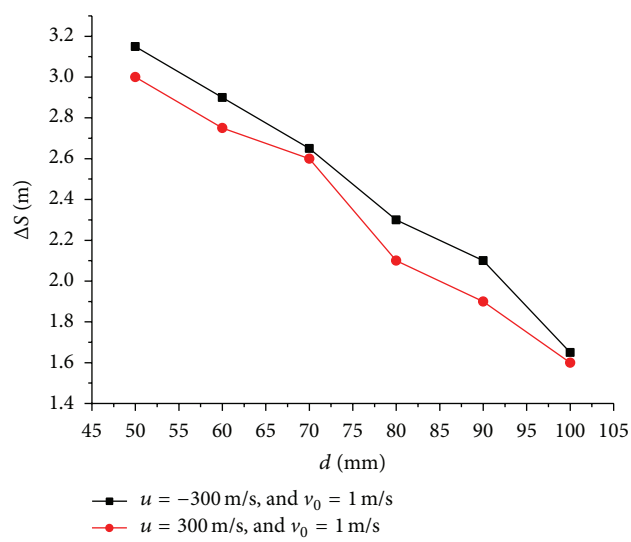

Figure 6: The relationship between particle diameter and separation distance under different direction airflow velocity (u = ±300 m/s, v_0 = +1 m/s).

As can be seen in Figure 6, separation distance decreases with the increase of particle diameter. It also can be concluded that the separation effect under airflow velocity −300 m/s is better than that under airflow velocity 300 m/s.

Table 2: Levels of factors.

Level	Factor		
	A gangue diameter d (mm)	B height difference h_p (m)	C conveyor belt velocity v_0 (m/s)
1	50	0.40	0.50
2	80	0.80	1.00
3	100	1.10	2.00

Table 3: Experimental results of separation effect.

Experiment number	A	B	C	Separation distance ΔS (m)	
				u and v_0 are in the opposite direction	u and v_0 are in the same direction
1	50	0.4	0.5	3.05	2.21
2	50	0.8	1.0	2.2	1.14
3	50	1.1	2.0	2.05	0.78
4	80	0.4	1.0	2.15	1.08
5	80	0.8	2.0	1.48	0.65
6	80	1.1	0.5	1.25	0.42
7	100	0.4	2.0	1.85	0.98
8	100	0.8	0.5	1.55	0.37
9	100	1.1	1.0	1.40	0.28

The separation effect also can be analyzed from (9); dynamic pressure difference ΔP_d can be expressed as $\rho(u^2-\dot{x}^2)/2$ when u and v_0 are in the same direction, while, when u and v_0 are in the opposite direction, the dynamic pressure difference ΔP_d can be expressed as $\rho(u^2+\dot{x}^2)/2$. Thus, it can be obtained from the above analysis that separation effect under airflow velocity −300 m/s is significantly better than that of under airflow velocity 300 m/s.

3.3. Orthogonal Experiment of Pneumatic Separation. Digital image processing technology has been used to identify the target of various patterns of coal and gangue in underground pneumatic separation system. Before mineral materials are sent to machine vision system, coal and gangue have been crushed to 100 mm by impact crusher. The size of materials is ranging from 50 mm to 100 mm. These materials are sent by the conveyor belt for coal and gangue digital image information identification (as shown in Figure 1).

In this study, separation distance ΔS (m) is selected as the primary index to evaluate the pneumatic separation effect. Pneumatic separation influenced by different airflow direction can be achieved by changing the arrangement of high-pressure value. The pneumatic separation test system mainly consists of conveyor belt, queuing system, machine vision system, control system, and high-pressure air injection system. When coal and gangue materials fell down from the conveyor belt, gangue will be identified by machine vision system, and the information is transported to control system through image sensor to drive the electromagnetic value open. Thus, coal gangue pneumatic separation is realized. The air compressor used in pneumatic separation testing system is LG-6.5/10, its working pressure is 1.0 Mpa, and certified capacity is 6.5 m^3/min.

From the analysis shown in Section 3, the conveyor velocity v_0, height difference h_p, and gangue diameter d are selected as the three factors. Factors and levels are listed in Table 2. According to the identified level of factors, orthogonal table L_9 (3^4) is applied in the test. Orthogonal experiment arrangement and results are shown in Table 3.

4. Result and Discussion

4.1. Variance Analysis and Range Analysis Based on Orthogonal Test. As can be seen from Table 2, each factor at different levels is approximate linearity, so the method of regression analysis is to obtain the linear function relationship between them appropriately [25]. Thus, the regression equations of coal gangue separation distance under different airflow direction are derived. Equation (25) represents the regression equation when u and v_0 are in the opposite direction, and (26) represents the regression equation when u and v_0 are in the same direction, where y is the separation distance of coal and gangue, x_1 represents the diameter of gangue, x_2 is the height difference, and x_3 is the velocity of conveyor belt:

$$y = 4.67 - 0.019x_1 - 1.773x_2 + 0.092x_3, \quad (25)$$

$$y = 3.60 - 0.02x_1 - 1.599x_2 - 0.14x_3. \quad (26)$$

Variance analysis is carried out on the regression equation to make significance test, and the results are shown in Tables 4 and 5. In order to determine the optimal pneumatic separation solutions, comparative analyses of the ranges between various levels of each factor are carried out. The range analysis is shown in Table 6.

In Table 6, subscripts 1 and 2 used in influence factors (A, B, C) represent the fact that u and v_0 are in the opposite

Table 4: Variance analysis (u and v_0 are in opposite direction).

Factor	Squariance	DOF	Mean square	F value
A	1.346	2	0.673	Distinctively
B	1.013	2	0.506	Distinctively
C	0.041	2	0.020	Distinctively
Regression	2.163	3	0.721	11.752
Error	0.307	5	0.061	
Sum	2.470	8		

Table 5: Variance analysis (u and v_0 are in the same direction).

Factor	Squariance	DOF	Mean square	F value
A	1.160	2	0.58	Distinctively
B	1.411	2	0.705	Distinctively
C	0.067	2	0.034	Distinctively
Regression	2.509	3	0.836	15.397
Error	0.272	5	0.054	
Sum	2.781	8		

direction and the same direction, respectively. K_{jm} ($m = 1, 2, \ldots, n$) is the sum of index values corresponding to factors in column j at level m. The value of K_{jm} determines the optimal level and combination of factors in column j. R_j reflects the ranges of the index with the variation of factors in column j, and the influence of the factor will be more significant if the value R_j is greater.

According to Tables 4 and 5, all the three factors mentioned above have significant influence on pneumatic separation distance. As shown in Table 6, the pneumatic separation distances ΔS are all decreasing with the increased value of the three factors. The analysis shows that gangue diameters have the most significant influence on separation distance.

4.2. Analysis of Experiment Results Based on Support Vector Machine (SVM). From the above analysis shown in Section 4.1, the significant degrees of different factors for separation distance are obtained by variance analysis. Besides, the primary and secondary relations of the influence factors with pneumatic separation distance could be obtained according to the range analysis. However, the optimal combination is a relative definition for the limited levels and has great one-sided characteristic. Most cases occurred in the experiment; the so-called "optimal combination of the factors" is a relative optimal, not the real optimal.

For further analysis of the experiment result, SVM [26–30] is introduced. The detailed functional forms of SVM are given in the Appendix. Optimization settings for factors that have influences on coal gangue pneumatic separation could be divided into the following steps: (1) collect the necessary data using orthogonal experiment; (2) set SVM learning model parameters and determine SVM kernel function; (3) input learning samples, and obtain parameters; (4) establish the fitting model according to parameters obtained above; (5) determine the levels of parameters in a certain range, and then combine these levels to establish a large number of input vector samples; (6) input vector sample into the fitting model and then obtain the output sample.

The relationship of separation distance ΔS and various influence factors is obtained through the above analysis. As shown in Figure 7, x- and y-axes represent two of the three influence parameters, respectively. 14 values equally spaced from the range of parameters of orthogonal experiment are taken, respectively. Thus, the comprehensive collection of the two parameters could form 196 samples, and the extreme value is selected in the third parameter in orthogonal experiment.

Figures 7(a) and 7(b) show the relationships of separation distance ΔS and the three factors when u and v_0 are in the opposite direction. As can be seen from Figures 7(a) and 7(b), pneumatic separation distance ΔS decreases with the increase of conveyor velocity v_0, the height difference h_p, and gangue diameter d. It also can be concluded that gangue diameter d has the greatest influence on separation distance ΔS.

Figures 7(c) and 7(d) have shown the relationships of separation distance ΔS and factors when u and v_0 are in the same direction. As can be seen from Figures 7(c) and 7(d), there is the same variation trend as that of Figures 7(a) and 7(b). Through the analysis of the two groups of figures, pneumatic separation effect will be better when u and v_0 are in the opposite direction. It can be concluded that the SVM intelligent model has important guiding significance and practical value for coal gangue pneumatic separation.

4.3. Correction of the Theoretical Formula. Based on the least square method, (23) and (24) in Section 3.2 can be transformed into a function of k_n and k_r parameters through variable substitution; then set up equations based on the experiments data. The result of k_n and k_r can be calculated finally.

When v_0 and u are in the same direction, nonlinear correction term can be given as $k_n = 0.0205$, and linear correction term $k_r = 1.1$. Thus, the formula can be expressed as

$$\begin{aligned}\Delta S &= S_i + S_{j1} + S_{f1} - S_0 \\ &= v_0\sqrt{\frac{2h_p}{g}} + \frac{m\ln\left(e^{(m\ln(u/v_0-1)-0.0205At_{j1}\rho u)/m}+1\right) - 2mu\ln\left(u/v_0\right) + At_{j1}\rho u}{2A\rho u} \\ &\quad + \frac{2h_f u e^{0.0205At_{j1}u\rho/m}}{\left(e^{\ln(u/v_0-1)} + e^{0.0205At_{j1}u\rho/m}\right)\left(gt_{j1}+2v_p\right)t_{j1}} - v_0\sqrt{\frac{2\left(h_p+h_j+h_f\right)}{g}} - 1.1.\end{aligned} \tag{27}$$

Table 6: Range analysis.

	A		B		C	
	A_1	A_2	B_1	B_2	C_1	C_2
K_{j1}	7.30	4.13	7.05	4.17	5.85	3.00
K_{j2}	4.88	2.15	5.23	2.16	5.75	2.49
K_{j3}	4.8	1.63	4.7	1.48	5.38	2.43
R_j	0.83	0.83	0.78	0.90	0.16	0.19

Table 7: Experimental and calculated results of separation effect.

Experiment number	Experiment value ΔS (m)	Calculated value $\Delta' S$ (m)	Error (%)	Experiment value ΔS (m)	Calculated value $\Delta' S$ (m)	Error (%)
	u and v_0 are in the same direction			u and v_0 are in opposite direction		
1	2.21	2.33	5.15	3.05	3.16	3.48
2	1.14	1.21	5.78	2.2	2.37	7.17
3	0.78	0.92	15.2	2.05	2.21	7.23
4	1.08	1.23	12.2	2.15	2.36	8.89
5	0.65	0.71	8.45	1.48	1.69	12.42
6	0.42	0.49	14.3	1.25	1.43	12.58
7	0.98	1.14	14.03	1.85	2.07	10.62
8	0.37	0.44	15.9	1.55	1.74	10.92
9	0.28	0.33	15.2	1.40	1.56	10.26

When v_0 and u are in the opposite directions, nonlinear correction term k_n and linear correction term k_r can be given as $k_n = 1.56 \times 10^5$ and $k_r = 4.4$. Thus, the formula is obtained as

$$\begin{aligned}\Delta S &= S_0 + S_{j2} + S_{f2} - S_i \\ &= v_0\sqrt{\frac{2\left(h_p + h_j + h_f\right)}{g}} \\ &\quad + \frac{2m\ln\left(\cos\left(\left(1.56\times10^5 A t_{j2} u\rho - 2m\arccos\left(u/\sqrt{v_0^2+u^2}\right)\right)/2m\right)\right) - 2m\ln\left(u/\sqrt{v_0^2+u^2}\right)}{A\rho} \\ &\quad + \tan\left(\frac{A t_{j2}\rho u - 2m\arccos\left(u/\sqrt{v_0^2+u^2}\right)}{2m}\right)\frac{2uh_f}{t_{j2}\left(g t_{j2} + 2v_p\right)} - v_0\sqrt{\frac{2h_p}{g}} - 4.4.\end{aligned} \tag{28}$$

In order to verify the effectiveness of theoretical formula, nine samples shown in Table 3 are selected as verification samples. The comparison of experiment results and calculated results is shown in Table 7.

As can be seen from Table 7, calculated value and experiment value of coal gangue pneumatic separation distance have high consistent degrees, the separation distance error between experiment value and calculated result is less for gangue with smaller diameter, and the separation distance error increases with the increase of gangue diameter. However, the separation distance error between experiment value and calculated result is still less than 16%. Thus, it can be concluded that (27) and (28) have important guiding significance and practical value for coal gangue pneumatic separation.

5. Conclusions

The established coal and gangue pneumatic separation model reflects the basis motion law of gangue affected by airflow and coal without being affected by airflow, which provides two feasible solutions for underground pneumatic separation

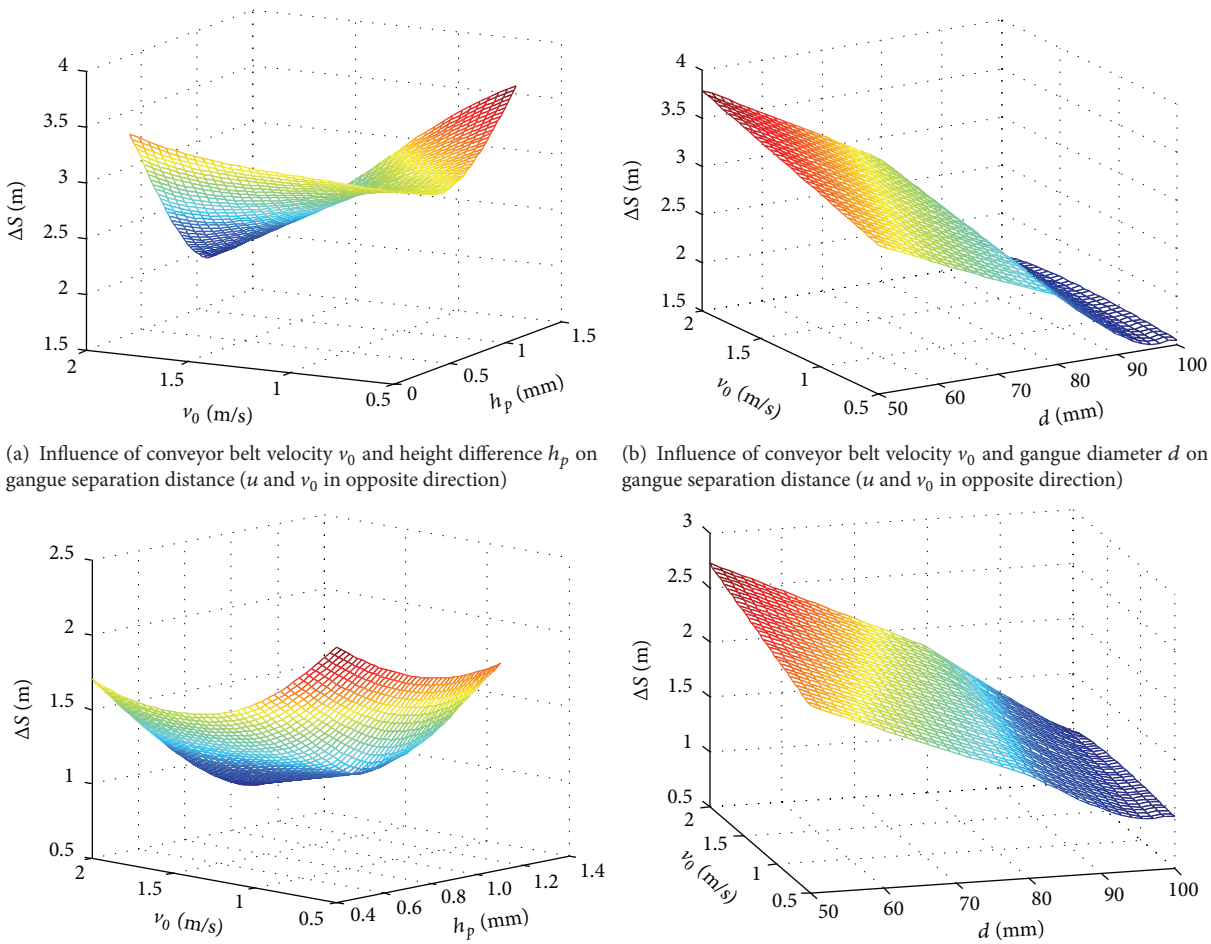

(a) Influence of conveyor belt velocity v_0 and height difference h_p on gangue separation distance (u and v_0 in opposite direction)

(b) Influence of conveyor belt velocity v_0 and gangue diameter d on gangue separation distance (u and v_0 in opposite direction)

(c) Influence of conveyor belt velocity v_0 and height difference h_p on gangue separation distance (u and v_0 in the same direction)

(d) Influence of conveyor belt velocity v_0 and gangue diameter d on gangue separation distance (u and v_0 in the same direction)

Figure 7: Influence of three factors on gangue separation distance.

under two kinds of arrangement scheme of high-pressure value. The analysis in theory is consistent with that obtained in the experiments, which validate the established theoretical model and present the following conclusions:

(1) Different high-pressure value arrangement schemes have great influence on gangue pneumatic separation, the theoretical formulas of coal gangue pneumatic separation distance affected by different airflow direction are derived, and the expressions of the two formulas are different under different airflow direction.

(2) A series of air-solid multiphase flow simulations and orthogonal experiments were conducted to clarify its effect under different airflow direction. Based on the analysis, pneumatic separation effect will be better under the condition of u and v_0 being in the opposite direction. Pneumatic separation distance ΔS decreases with the increased values of the three factors (conveyor velocity v_0, height difference h_p, and gangue diameter d). These analyses also show that gangue diameters have the most significant influence on separation distance, followed by conveyor velocity v_0 and height difference h_p.

(3) The relationship of pneumatic separation distance ΔS and influence factors was obtained by SVM intelligent model; the theoretical formulas of coal gangue pneumatic separation distance are corrected based on the analysis of orthogonal experiment data. The corrected formula is suitable to serve as the theory basis of coal gangue pneumatic separation.

Appendix

Mathematical Quantity for Support Vector Machine Analysis

Original research based on SVM was originally used in linear fitting problem. If function $f(x)$ appears with linear function characteristics, it can be expressed as $y = \boldsymbol{\omega}\mathbf{x} + b$. Assume that all the data $(\mathbf{x}_i, \mathbf{y}_i)$ $(i = 1, 2, \ldots, n)$, $x \in R^l$ (R^l is the real of l degree), and $y \in R$. Function y can be fitted by linear function $y = \boldsymbol{\omega}\mathbf{x} + b$ in precision ε,

$$\left|\mathbf{y}_i - \boldsymbol{\omega}\mathbf{x}_i - b\right| \leq \varepsilon, \tag{A.1}$$

where $\mathbf{x}_i$ is the input vector, $\mathbf{y}_i$ is a real constant as the output vector, $\boldsymbol{\omega}$ is a normal vector for fitting function, b is threshold value, and ε is the fitting precision.

Based on the principle of minimum structural risk, the optimization objective could achieve better generalization ability at the minimum value of $\|w\|^2/2$. Considering the existence of approximation error ξ (ξ is a real constant) in actual application, therefore, SVM can be expressed as

$$\begin{aligned} \min \quad & \frac{1}{2}w^2 + C\sum_{i=1}^{n}(\xi_i + \xi_i^*) \\ \text{s.t.} \quad & y_i - wx - b \le \varepsilon + \xi_i \\ & wx_i + b - y_i \le \varepsilon + \xi_i^* \\ & \xi_i \ge 0,\ \xi_i^* \ge 0, \end{aligned} \tag{A.2}$$

where C is balance factor, which is used to control the degree of punishment beyond the error sample, and ξ_i and ξ_i^* are relaxation factors. ξ_i and ξ_i^* are of the same nature; in general, relaxation factor at the top of fitting curve is recorded as ξ_i; conversely, it is recorded as ξ_i^*.

Equation (28) could change into quadratic programming problem based on dual theory. Then the Lagrange equation is established:

$$\begin{aligned} & L(w, b, \xi_i, \xi_i^*, \alpha_i, \alpha_i^*, \eta_i, \eta_i^*) \\ & = \frac{1}{2}w^2 + C\sum_{i=1}^{\alpha}(\xi_i + \xi_i^*) \\ & \quad - \sum_{i=1}^{\alpha}\alpha_i(\varepsilon + \xi_i - y_i + wx_i + b) \\ & \quad - \sum_{i=1}^{\alpha}\alpha_i^*(\varepsilon + \xi_i^* + y_i - wx_i - b) \\ & \quad - \sum_{i=1}^{\alpha}(\eta_i\xi_i + \eta_i^*\xi_i^*), \end{aligned} \tag{A.3}$$

where parameters α_i and α_i^* are Lagrange multiplier, $\alpha_i \gg 0$, $\alpha_i^* \gg 0$, and η_i and η_i^* are temporary variables, $\eta_i \gg 0$, $\eta_i^* \gg 0$. α_i and α_i^* have the same physical significance with η_i and η_i^*.

The optimal solution of (A.1) could be derived by calculating the saddle points of the Lagrange equation. Thus, function approximation problem can be obtained:

$$\begin{aligned} w &= \sum_{x_i \in S_{SV}}(\alpha_i - \alpha_i^*)x_i, \\ f(x) &= wx + b = \sum_{x_i \in S_{SV}}(\alpha_i - \alpha_i^*)(x_i \cdot x) + b, \end{aligned} \tag{A.4}$$

where S_{SV} in (A.4) is the SVM and the training sample is the support vector when $(\alpha_i - \alpha_i^*)$ is not equal to zero.

Conflict of Interests

The authors declare that there is no conflict of interests regarding the publication of this paper.

Acknowledgments

Financial support for this work, provided by National High-Tech Research and Development Program of China (863 Program) (no. 2012AA062102), Innovation Training Project of Graduate Student in Jiangsu Province (CXLX13_936), and the Priority Academic Program Development of Jiangsu Higher Education Institutions (PAPD), is gratefully acknowledged.

References

[1] M. G. Qian, J. L. Xu, and X. X. Miao, "Technique of cleaning mining in coal mine," *Journal of China University of Mining & Technology*, vol. 32, pp. 343–348, 2003.

[2] J.-X. Zhang and X.-X. Miao, "Underground disposal of waste in coal mine," *Journal of China University of Mining & Technology*, vol. 35, no. 2, pp. 197–200, 2006.

[3] C. S. Dong, P. X. Yao, and Z. H. Liu, "Hydraulic automatic separation technology of coal and refuse in underground mine," *Coal Science and Technology*, vol. 35, no. 3, pp. 54–56, 2007.

[4] J. Li, D. Yang, and C. Du, "Evaluation of an underground separation device of coal and gangue," *International Journal of Coal Preparation and Utilization*, vol. 33, no. 4, pp. 188–193, 2013.

[5] C. Luo, C. Du, L. Xu, and K. Zheng, "Fractal distribution studies of a rotary crushing mechanism," *Recent Patents on Mechanical Engineering*, vol. 7, no. 1, pp. 44–51, 2014.

[6] J.-P. Li, C.-L. Du, and L.-J. Xu, "Impactive crushing and separation experiment of coal and gangue," *Journal of the China Coal Society*, vol. 36, no. 4, pp. 687–690, 2011.

[7] S. Al-Thyabat and N. J. Miles, "An improved estimation of size distribution from particle profile measurements," *Powder Technology*, vol. 166, no. 3, pp. 152–160, 2006.

[8] J. Tessier, C. Duchesne, and G. Bartolacci, "A machine vision approach to on-line estimation of run-of-mine ore composition on conveyor belts," *Minerals Engineering*, vol. 20, no. 12, pp. 1129–1144, 2007.

[9] T. Andersson, M. J. Thurley, and J. E. Carlson, "A machine vision system for estimation of size distributions by weight of limestone particles," *Minerals Engineering*, vol. 25, no. 1, pp. 38–46, 2012.

[10] S. Al-Thyabat, N. J. Miles, and T. S. Koh, "Estimation of the size distribution of particles moving on a conveyor belt," *Minerals Engineering*, vol. 20, no. 1, pp. 72–83, 2007.

[11] E. Hamzeloo, M. Massinaei, and N. Mehrshad, "Estimation of particle size distribution on an industrial conveyor belt using image analysis and neural networks," *Powder Technology*, vol. 261, pp. 185–190, 2014.

[12] Y. K. Yen, C. L. Lin, and J. D. Miller, "Particle overlap and segregation problems in on-line coarse particle size measurement," *Powder Technology*, vol. 98, no. 1, pp. 1–12, 1998.

[13] C. L. Lin, Y. K. Yen, and J. D. Miller, "Plant-site evaluations of the OPSA system for on-line particle size measurement from moving belt conveyors," *Minerals Engineering*, vol. 13, no. 8, pp. 897–909, 2000.

[14] C. Aldrich, G. T. Jemwa, J. C. van Dyk, M. J. Keyser, and J. H. P. Van Heerden, "Online analysis of coal on a conveyor belt by use of machine vision and kernel methods," *International Journal of Coal Preparation and Utilization*, vol. 30, no. 6, pp. 331–348, 2010.

[15] J. X. Zhang, T. Chen, Z. D. Yu, and W. Li, "Xinjiang cotton seed color separation system based on computer vision," *Transactions of the Chinese Society of Agricultural Machinery*, vol. 40, no. 10, pp. 161–164, 2009.

[16] C. Guo, H. Wang, W. Liang, J. G. Fu, and X. Yi, "Liberation characteristic and physical separation of printed circuit board (PCB)," *Waste Management*, vol. 31, no. 9-10, pp. 2161–2166, 2011.

[17] M. Xu, G. M. Li, J. Yin, and W. Z. He, "Crushing and pneumatic separation of printed circuit board scraps," *Environmental Science & Technology*, vol. 30, pp. 72–74, 2007.

[18] V. Kumar, J.-C. Lee, J. Jeong, M. K. Jha, B.-S. Kim, and R. Singh, "Novel physical separation process for eco-friendly recycling of rare and valuable metals from end-of-life DVD-PCBs," *Separation and Purification Technology*, vol. 111, pp. 145–154, 2013.

[19] V. Kumar, J.-C. Lee, J. Jeong, M. K. Jha, B.-S. Kim, and R. Singh, "Recycling of printed circuit boards (PCBs) to generate enriched rare metal concentrate," *Journal of Industrial and Engineering Chemistry*, vol. 21, pp. 805–813, 2015.

[20] N. Hayashi and T. Oki, "Effect of orifice introduction on the pneumatic separation of spherical particles," *Materials Transactions*, vol. 55, no. 4, pp. 700–707, 2014.

[21] T. Havlik, D. Orac, M. Berwanger, and A. Maul, "The effect of mechanical-physical pretreatment on hydrometallurgical extraction of copper and tin in residue from printed circuit boards from used consumer equipment," *Minerals Engineering*, vol. 65, pp. 163–171, 2014.

[22] Z. Liu, Y. Xie, Y. Wang, J. Yu, S. Gao, and G. Xu, "Tandem fluidized bed elutriator—pneumatic classification of coal particles in a fluidized conveyer," *Particuology*, vol. 10, no. 5, pp. 600–606, 2012.

[23] G.-H. Yang, D.-C. Zheng, J.-H. Zhou, Y.-M. Zhao, and Q.-R. Chen, "Air classification of moist raw coal in a vibrated fluidized bed," *Minerals Engineering*, vol. 15, no. 8, pp. 623–625, 2002.

[24] X. Yang, Z. Fu, J. Zhao, E. Zhou, and Y. Zhao, "Process analysis of fine coal preparation using a vibrated gas-fluidized bed," *Powder Technology*, vol. 279, pp. 18–23, 2015.

[25] K. T. Fang, C. X. Ma, and J. K. Li, "Recent development of orthogonal factorial designs and their applications—applications of regression analysis to orthogonal designs," *Application of Statistics and Management*, vol. 18, pp. 44–49, 1999.

[26] X. H. Guo and X. P. Ma, "Support vector machine toolbox in Matlab environment," *Computer Applications and Software*, vol. 24, no. 12, pp. 57–59, 2007.

[27] X. Fang, Z.-J. Ding, and X.-Q. Shu, "Hydrogen yield prediction model of hydrogen production from low rank coal based on support vector machine optimized by genetic algorithm," *Journal of the China Coal Society*, vol. 35, no. 1, pp. 205–209, 2010.

[28] Y. Q. Qiu, G. H. Hu, and W. L. Pan, "Parallel algorithm of support vector machine based on orthogonal array," *Journal of Yunnan University*, vol. 28, no. 2, pp. 93–97, 2006.

[29] J. A. K. Suykens and J. Vandewalle, "Least squares support vector machine classifiers," *Neural Processing Letters*, vol. 9, no. 3, pp. 293–300, 1999.

[30] J. A. K. Suyken and J. Vandewalle, "Sparse least squares Support Vector Machine classifiers," in *Proceedings of the 8th European Symposium on Artificial Neural Networks (ESANN '00)*, pp. 37–42, Bruges, Belgium, April 2000.